Efficient vibro-acoustic identification of boundary conditions by low-rank parametric model order reduction

S. van Ophem[a,b,*], A. van de Walle[a,b], E. Deckers[a,b], W. Desmet[a,b]

[a] *KU Leuven, Department of Mechanical Engineering, Celestijnenlaan 300 B, B-3001, Heverlee, Belgium*
[b] *DMMS lab, Flanders Make*

Abstract

A novel method is presented that detects the proper boundary conditions of a test setup in a short time period by combing numerical models with experimental data. This allows for detection and localization of possible anomalies in the assumed boundary conditions of the system. The method works by combining a low-rank parametric model order reduction technique with a model updating strategy, where the boundary conditions of a numerical finite element model are updated by using frequency response function data. This combination makes it possible to update a large amount of parameters, because the assumed low-rank nature of the changes enables the use of non-parametric model order reduction techniques for the calculation of the reduced basis. This is possible, because the system can be rewritten in such a way that the parameter dependencies only show up in the feed-forward matrix of the system, thus no *a-priori* sampling of the parameter space is required. Thus, the resulting model can identify a large amount of parameters, including the identification of local changes in the boundary conditions. The method is validated with a test-setup in which an aluminum plate is attached to an acoustic cavity and the boundary conditions are varied gradually, by removing the bolts that are clamping the plate. By applying the proposed model updating scheme to the rotational stiffness along the edge in combination with an additional damping term, it is shown that the proposed method can detect which bolts are removed and also leads to a good match in the frequency response functions. Moreover, it is shown that these results are achieved in only a few minutes, in contrast to the same procedure with full order models.

Keywords: Parametric model order reduction, Model updating, Vibro-acoustics, Finite element method, Low-rank parametric model order reduction, Boundary conditions

1. Introduction

The advancement of computer power in the last decades has led to the increased usage of numerical calculation software for predicting the vibro-acoustic behavior of structures,

*Corresponding author
Email address: Sjoerd.vanOphem@kuleuven.be (S. van Ophem)

with schemes like the Finite Element Method (FEM) [1] and the Boundary Element Method [2]. When it is desired to use a numerical model in conjunction with measurements, it is important that the numerical model matches the real system to a certain degree. Since it is generally difficult to know all the parameters in the numerical model *a-priori*, model updating has risen as a viable tool to iteratively update the numerical model to a required accuracy [3], which usually means that the difference between measured data and the numerical model is minimized. Model updating approaches can be based on mode shapes, eigenfrequencies and frequency response functions (FRFs) [3], [4] and can work both in the time and frequency domain [5]. The model updating procedure can be used for a wide range of engineering problems, for example boundary detection [6], damage detection [7] and shape identification [8]. Generally, many system evaluations are necessary to obtain the optimal model. Since the used numerical models are usually computationally demanding, it would be beneficial to implement Model Order Reduction (MOR) techniques to speed up the calculations, such as modal reduction [9], balanced truncation [10], proper orthogonal decomposition [11] and techniques based on Krylov subspace projection [12], [13]. This paper focuses on Krylov techniques, because of their ability to handle the large, sparse, linear systems that result from vibro-acoustic FE models [14], [15], but the proposed method would also work with other projection based model reduction techniques.

When MOR is used for a parameter study, it is desirable to maintain the parameter dependency in either the reduced model, or in the reduced basis used for calculating the Reduced Order Model (ROM). Otherwise, the reduced basis has to be recalculated for every change in parameter values, which requires expensive full system inversions. To avoid this, parametric model order reduction (pMOR) techniques have been developed [16]. Most of these techniques are based on sampling the parameter space, which means that the range of the parameters has to be known *a-priori*, and that the accuracy of the reduced model cannot be guaranteed outside of the sampled parameter range. When a large amount of parameters has to be retained, which occurs when strongly localized or spatially distributed parameters have to be detected, and each of these parameters is sampled at several parameter values, the construction of the reduced basis might take too long. Thus in practice the amount of parameters in the ROM is restricted. Recently, it was found by multiple authors [17], [18], that under certain low-rank assumptions of the parameter dependence no *a-priori* sampling of the parameter space has to be performed to calculate the projection matrix. This can be done by remodeling them as additional localized inputs to the system with extra input vectors that indicate the positions at which the low-rank parameter applies. This means that non-parametric multiple input algorithms for calculating the reduced basis can be used. The result is only a single reduced basis that can be used for all parameter variations. Since no *a-priori* sampling has to be applied, a large amount of parameter dependencies can be accounted for by simply increasing the amount of inputs. Also, as has been shown in [19], if the parameters have any correlation in their behavior, which is often the case for dynamic systems, this redundancy can be removed and the size of the ROM stays small, in spite of the many inputs. This methodology has been extended to second order systems in [19].

In this paper model updating is used to determine the structural Boundary Conditions (BCs) of a vibro-acoustic system. While structural BCs are usually modeled as clamped, simply-supported or free, in practice these boundary conditions are never truly satisfied [20]. Since the dynamic behavior of a structure is highly dependent on the BCs, it would

be beneficial to have a numerical tool that detects whether the boundary conditions that are assumed in the numerical model match the boundary conditions of the structure and warn the end user about possible discrepancies between the assumed BCs and the actual BCs. The main contribution of this paper is that it derives a methodology that can determine discrepancies and changes in the BCs in a short time frame. The paper is split in two parts: The first part in Secs. 2-3 describes a generic combined low rank pMOR and model updating procedure, that can efficiently determine the BCs of several vibro-acoustic systems. The described method can handle low-rank changes in the mass, the damping and the stiffness matrix and includes the analytical derivatives, required for the model updating procedure. The second part in Sec. 4 demonstrates the usage and effectiveness of the method with a specific vibro-acoustic example that utilizes measured FRF data of a clamped plate connected to an acoustic cavity. To establish whether the method can find differences in BCs, one of the edges of the plate is gradually loosened by removing the bolts that are clamping down the plate at the edges. The corresponding rotational stiffness and possible increase in damping of the edge is determined with model updating. It is shown that the method cannot only effectively estimate the areas of reduced stiffness and FRFs, but also that it achieves this in a short time span, as opposed to the same procedure with FRFs of the full model.

2. Low rank parametric model order reduction scheme

To speed-up the model updating process a pMOR scheme is used. The chosen scheme is the second order low-rank scheme as has recently been derived in [19]. This scheme makes it possible to reformulate the parametric system to an equivalent system that can be reduced with non-parametric model reduction techniques. Although the scheme has originally been derived in the time domain, a conversion to the frequency domain is straightforward by using the Laplace transform, as is shown in Sec. 2.2.

2.1. pMOR formulation in the time domain

As described in [19], the following parametric system description is used:

$$M(r)\ddot{\boldsymbol{x}}(t) + C(q)\dot{\boldsymbol{x}}(t) + K(p)\boldsymbol{x}(t) = \boldsymbol{b}_0 u(t), \tag{1}$$

$$\boldsymbol{y}_0(t) = L_0\boldsymbol{x}(t) + \boldsymbol{d}_0 u(t), \tag{2}$$

in which $M(r) \in \mathbb{R}^{n\times n}$ is the mass matrix, $C(q) \in \mathbb{R}^{n\times n}$ is the damping matrix, $K(p) \in \mathbb{R}^{n\times n}$ is the stiffness matrix, $\boldsymbol{b}_0 \in \mathbb{R}^{n\times 1}$ is the input vector, $L_0 \in \mathbb{R}^{n\times n}$ is the output matrix, $\boldsymbol{x}(t) \in \mathbb{R}^{n\times 1}$ describes the physical state (pressure, displacement, etc...), $u(t)$ is the input signal and $\boldsymbol{d}_0 \in \mathbb{R}^{n\times 1}$ is the feed-forward matrix, which is zero in this case. The parameter dependency in the system matrices $M(r)$, $C(q)$ and $K(p)$ is assumed to be affine and of low rank:

$$M(r) = M_0 + \sum_{m=1}^{\xi} r^{(m)} \boldsymbol{f}_m \boldsymbol{g}_m^T, \tag{3}$$

$$C(q) = C_0 + \sum_{l=1}^{\mu} q^{(l)} \boldsymbol{d}_l \boldsymbol{e}_l^T, \tag{4}$$

$$K(p) = K_0 + \sum_{k=1}^{\nu} p^{(k)} \boldsymbol{b}_k \boldsymbol{c}_k^T. \tag{5}$$

The matrices M_0, C_0 and $K_0 \in \mathbb{R}^{n\times n}$ are the parameter independent parts of $M(r)$, $C(q)$ and $K(p)$. The low rank changes are described by a vector-vector multiplication of the unit-vectors $\boldsymbol{b}_k$, $\boldsymbol{c}_k$, $\boldsymbol{d}_l$, $\boldsymbol{e}_l$, $\boldsymbol{f}_m$, $\boldsymbol{g}_m$, $\in \mathbb{R}^{n\times 1}$, thus leading to a matrix of rank-1. The system is rewritten by defining the following auxiliary inputs:

$$u_k^{(1)} = -p^{(k)} \boldsymbol{c}_k^T \boldsymbol{x}(t), \text{ for } k = 1, \dots \nu, \tag{6}$$

$$u_l^{(2)} = -q^{(l)} \boldsymbol{e}_l^T \dot{\boldsymbol{x}}(t), \text{ for } l = 1, \dots \mu, \tag{7}$$

$$u_m^{(3)} = -r^{(m)} \boldsymbol{g}_m^T \ddot{\boldsymbol{x}}(t), \text{ for } m = 1, \dots \xi. \tag{8}$$

This results in the extended input vector

$$\boldsymbol{u}_{ext}(t) = \begin{bmatrix} u_0(t) \\ \boldsymbol{u}^{(1)}(t) \\ \boldsymbol{u}^{(2)}(t) \\ \boldsymbol{u}^{(3)}(t) \end{bmatrix} \in \mathbb{R}^{1+\nu+\mu+\xi}, \tag{9}$$

with

$$\boldsymbol{u}^{(1)}(t) = \begin{bmatrix} u_1^{(1)}(t) \\ \vdots \\ u_\nu^{(1)}(t) \end{bmatrix}, \; \boldsymbol{u}^{(2)}(t) = \begin{bmatrix} u_1^{(2)}(t) \\ \vdots \\ u_\mu^{(2)}(t) \end{bmatrix}, \; \boldsymbol{u}^{(3)}(t) = \begin{bmatrix} u_1^{(3)}(t) \\ \vdots \\ u_\xi^{(3)}(t) \end{bmatrix}. \tag{10}$$

Also the input matrix is redefined as follows:

$$B_{ext} = \begin{bmatrix} \boldsymbol{b}_0 & \boldsymbol{b} & \boldsymbol{d} & \boldsymbol{f} \end{bmatrix} \in \mathbb{R}^{n\times(1+\nu+\mu+\xi)}, \tag{11}$$

with

$$\begin{aligned} \boldsymbol{b} &= \begin{bmatrix} \boldsymbol{b}_1 & \dots & \boldsymbol{b}_\nu \end{bmatrix} \in \mathbb{R}^{n\times\nu}, \\ \boldsymbol{d} &= \begin{bmatrix} \boldsymbol{d}_1 & \dots & \boldsymbol{d}_\mu \end{bmatrix} \in \mathbb{R}^{n\times\mu}, \\ \boldsymbol{f} &= \begin{bmatrix} \boldsymbol{f}_1 & \dots & \boldsymbol{f}_\xi \end{bmatrix} \in \mathbb{R}^{n\times\xi}. \end{aligned} \tag{12}$$

By shifting all the parameter dependent terms of Eq. (1) to the right-hand side, and utilizing the extended input matrix in Eq. (11) and extended inputs in Eq. (9), the system equation can be rewritten as follows:

$$M_0\ddot{\boldsymbol{x}}(t) + C_0\dot{\boldsymbol{x}}(t) + K_0\boldsymbol{x}(t) = B_{ext}\boldsymbol{u}_{ext}(t). \tag{13}$$

Correspondingly, the output equation is rewritten as follows:

$$\boldsymbol{y}_{ext}(t) = L_{ext}\boldsymbol{x}_{ext}(t) + D_{ext}(p,q,r)\boldsymbol{u}_{ext}(t), \tag{14}$$

with

$$\boldsymbol{y}_{ext} = \begin{bmatrix} \boldsymbol{y}_0 \\ y_1 \\ \vdots \\ y_\tau \end{bmatrix},\ L_{ext} = \begin{bmatrix} L_0 & 0 & 0 \\ \boldsymbol{c}^T & \boldsymbol{e}^T & \boldsymbol{g}^T \end{bmatrix},\ \boldsymbol{x}_{ext}(t) = \begin{bmatrix} \boldsymbol{x}(t) \\ \dot{\boldsymbol{x}}(t) \\ \ddot{\boldsymbol{x}}(t) \end{bmatrix}, \tag{15}$$

Moreover

$$\begin{aligned} \boldsymbol{c} &= \begin{bmatrix} \boldsymbol{c}_1 & \dots & \boldsymbol{c}_\nu \end{bmatrix} \in \mathbb{R}^{n\times\nu}, \\ \boldsymbol{e} &= \begin{bmatrix} \boldsymbol{e}_1 & \dots & \boldsymbol{e}_\mu \end{bmatrix} \in \mathbb{R}^{n\times\mu}, \\ \boldsymbol{g} &= \begin{bmatrix} \boldsymbol{g}_1 & \dots & \boldsymbol{g}_\xi \end{bmatrix} \in \mathbb{R}^{n\times\xi}. \end{aligned} \tag{16}$$

The consistency in the dimensions of Eq. (15) is guaranteed by extending the matrices $\boldsymbol{c}$, $\boldsymbol{e}$ and $\boldsymbol{g}$ with extra rows of zeros, so that the matrix $L_{ext} \in \mathbb{R}^{(\tau+n)\times 3n}$, in which $\tau = \max(\nu,\mu,\xi)$. Finally, the feed-forward matrix is extended as follows:

$$D_{ext}(p,q,r) = \begin{bmatrix} 0 & 0 & 0 & 0 \\ 0 & D^{(1)}(p) & D^{(2)}(q) & D^{(3)}(r)f \end{bmatrix},\ \in \mathbb{R}^{(n+\tau)\times(1+\nu+\mu+\xi)} \tag{17}$$

with

$$\begin{aligned} D^{(1)}(p) &= \mathrm{diag}(1/p^{(1)},\dots,1/p^{(\nu)}) \in \mathbb{R}^{\nu\times\nu}, \\ D^{(2)}(q) &= \mathrm{diag}(1/q^{(1)},\dots,1/q^{(\mu)}) \in \mathbb{R}^{\mu\times\mu}, \\ D^{(3)}(r) &= \mathrm{diag}(1/r^{(1)},\dots,1/r^{(\xi)}) \in \mathbb{R}^{\xi\times\xi}. \end{aligned} \tag{18}$$

By rewriting the system in such a form, outputs $y_1(t) = \dots = y_\nu = 0$, thus the resulting system gives the same output as Eq. (2). Furthermore, the parameter dependency only occurs in the feed-forward matrix (Eq. 17).

2.2. pMOR formulation in the frequency domain

By applying the Laplace transform on Eqs. (13), (14) the system can be transformed to the frequency domain. Applying the Laplace transform on Eq. (13), with Laplace variable $s = i\omega$, gives

$$M_0 s^2\boldsymbol{X}(s) + C_0 s\boldsymbol{X}(s) + K_0\boldsymbol{X}(s) = B_{ext}\boldsymbol{U}_{ext}(s), \tag{19}$$

with the following auxiliary inputs

$$U_k^{(1)} = \quad -p^{(k)} \boldsymbol{c}_k^T \boldsymbol{X}(s), \text{ for } \; k = 1, \ldots \nu, \tag{20}$$

$$U_l^{(2)} = \quad -q^{(l)} \boldsymbol{e}_l^T s\boldsymbol{X}(s), \text{ for } \; l = 1, \ldots \mu, \tag{21}$$

$$U_m^{(3)} = -r^{(m)} \boldsymbol{g}_m^T s^2 \boldsymbol{X}(s), \text{ for } m = 1, \ldots \xi. \tag{22}$$

The extended input vector $\boldsymbol{U}_{ext}$ can be defined in a similar fashion as in the time domain (Eqs. (9), (10), (11)). Rewriting Eq. (14) leads to

$$\boldsymbol{Y}_{ext}(s) = L_{ext} \boldsymbol{X}_{ext}(s) + D_{ext} \boldsymbol{U}_{ext}(s), \tag{23}$$

with

$$\boldsymbol{X}_{ext}(s) = \begin{bmatrix} \boldsymbol{X}(s) \\ s\boldsymbol{X}(s) \\ s^2\boldsymbol{X}(s) \end{bmatrix}, \; \boldsymbol{Y}_{ext}(s) = \begin{bmatrix} \boldsymbol{Y}_0(s) \\ Y_1(s) \\ \vdots \\ Y_\nu(s) \end{bmatrix}. \tag{24}$$

Filling in these expressions leads to the conclusion that all the outputs, expect for $Y_0(s)$ are zero:

$$Y_1(s) = \ldots = Y_\nu(s) = 0. \tag{25}$$

2.3. Reduced system matrices

Since Eq. (19) and (23) only contain parameter independent matrices, except for the feed-forward matrix, a non-parametric MOR technique, such as the Second Order Arnoldi (SOAR) scheme [12] can be used to calculate the reduced basis. This scheme calculates the reduced basis $V \in \mathbb{C}^{n \times r}$ with a moment matching procedure that enables the projection of the system matrices on a Krylov subspace of size r, as follows:

$$\begin{aligned} \hat{M}_0 &= V^T M_0 V, \; \hat{C}_0 = V^T C_0 V, \; \hat{K}_0 = V^T K_0 V, \\ \hat{B}_{ext} &= V^T B_{ext}, \; \hat{L}_{ext} = L_{ext} \begin{bmatrix} V & 0 & 0 \\ 0 & V & 0 \\ 0 & 0 & V \end{bmatrix}. \end{aligned} \tag{26}$$

More details about Krylov subspaces and moment matching can be found in [13]. From Eq. (11) and (15), the following reduced vectors follow:

$$\begin{aligned} \hat{\boldsymbol{b}}_k &= V^T \boldsymbol{b}_k, \; \hat{\boldsymbol{d}}_l = V^T \boldsymbol{d}_l, \; \hat{\boldsymbol{f}}_m = V^T \boldsymbol{f}_m, \\ \hat{\boldsymbol{c}}_k^T &= \boldsymbol{c}_k^T V, \; \hat{\boldsymbol{e}}_l^T = \boldsymbol{e}_l^T V, \; \hat{\boldsymbol{g}}_m^T = \boldsymbol{g}_m^T V. \end{aligned} \tag{27}$$

Since $\hat{Y}_1(s) = \ldots = \hat{Y}_\nu(s) = 0$, the following pMOR formulation can be recovered:

$$
\begin{aligned}
(-\omega^2 \hat{M}(r) + i\omega \hat{C}(q) + \hat{K}(p))\hat{\boldsymbol{X}}(\omega) &= \hat{B}_0 \boldsymbol{U}(\omega) \\
\hat{K}_{dyn}(p,q,r,\omega)\hat{\boldsymbol{X}}(\omega) &= \hat{B}_0 \boldsymbol{U}(\omega). \qquad (28)
\end{aligned}
$$

Thus the reduced basis of the parametric system can be calculated without sampling the parameter space, which is a significant advantage when a large amount of parameters have to be retained in the reduced basis.

3. Model updating procedure

Starting from a model that adheres to the assumptions made in Sec. 2, the goal of the model updating procedure is to find the values of the local parameters that minimize the following cost function:

$$
\arg \min_{\log_{10}(\boldsymbol{p})} \log_{10} \left(\sum_{l=1}^{n_{freq}} (T_n^l - T_e^l)^2 + \sum_{k=1}^{\nu} \eta (p^{(k)} - p_{init}^{(k)})^2 \right), \qquad (29)
$$

with

$$
\begin{aligned}
T_e^l &= 20 \log_{10} \left(\left| \frac{X_e(\omega_l)}{F_e(\omega_l)} \right| \right), \qquad (30) \\
T_n^l &= 20 \log_{10} \left(\left| \frac{X_n(\omega_l, \log_{10}(\boldsymbol{p}))}{F_n(\omega_l, \log_{10}(\boldsymbol{p}))} \right| \right). \qquad (31)
\end{aligned}
$$

In these equations T_e^l represents the experimentally measured FRF at frequency ω_l and T_n^l the FRF from the numerical model, and the force is defined as $F(\omega_l) = B_0 U(\omega_l)$. For ease of notation, the cost function has only been described as a function of parameter vector $\boldsymbol{p}$, but an extension to the full parameter space is straightforward. The first term in Eq. (29) minimizes the differences between the measured FRF and the FRF from the numerical model for a number of selected frequency points. These frequency points should be chosen around the resonances, so that the influence of noise is minimized. The second term is a Tikhonov regularization term [21] that reduces the effect of ill-conditioning and can be adjusted with parameter η. As can be seen in Eq. (29), also an extra parameter $p_{init}^{(k)}$ is introduced: This parameter represents the initial values of the parameters that are estimated. Furthermore, as can be observed in Eq. (31), the logarithm of the parameters is used, because it allows for modeling variables with a large dynamic range.

The used model updating procedure is similar to the one described in [22] and [23]: It consists of an inverse method using quasi-Newton optimization to obtain the parameter values that minimize the cost function in Eq. (29). The quasi Newton method that is applied here is the Broyden-Fletcher-Goldfarb-Shanno (BFGS) method [24], that approximates the Hessian matrix in an efficient way. Since the BFGS method requires a positive definite approximation of the Hessian matrix, a steepest descent method is used when this condition is not met. For the required line search algorithm a scheme based on the Armijo-Goldstein condition is used [25].

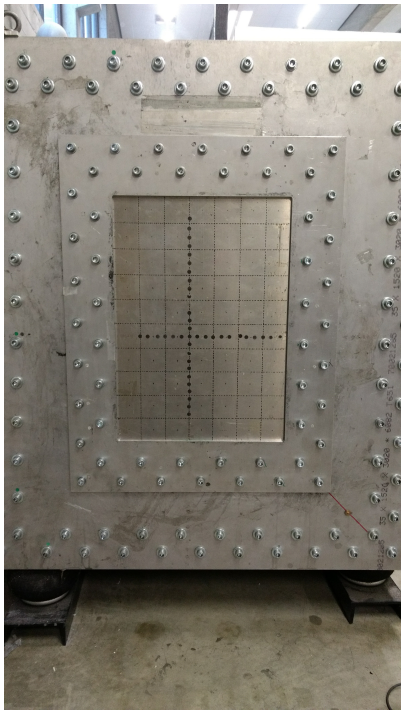

Figure 1: The SoundBox.

3.1. Calculation of the gradient

Besides the pMOR procedure, an additional speed-up of the calculation time is obtained by calculating the analytical expressions of the gradient of the cost function to the parameters, instead of using finite differences to approximate them. To calculate the gradient of the cost function to the parameters, the derivative of the field variables to the parameter values has to be known first. This derivative is given by

$$\frac{\partial X(p,\omega)}{\partial p_j} = -K_{dyn}^{-1}(p,\omega)\frac{\partial K_{dyn}(p,\omega)}{\partial p_j}K_{dyn}^{-1}(p,\omega)\boldsymbol{F}(\omega). \tag{32}$$

This expression can be substituted in the derivative of the cost function to the parameter, which is shown in Appendix A. The resulting matrix inverses, that are described in more detail in Sec. 4.1, have to be calculated only once per frequency line for every optimization step, in contrast to the numerical approach with finite differences. For an additional speedup in the gradient calculations, an adjoint formulation can be considered, such as described in [26].

Microphone number	$x\ [m]$	$y\ [m]$	$z\ [m]$
1	0.6	0.5	0.05
2	0.4	0.5	0.05
3	0.2	0.5	0.05
4	0.55	0.29	0.535
5	0.35	0.29	0.535
6	0.15	0.29	0.535
7	0.5	0.607	0.82
8	0.3	0.607	0.82
9	0.783	0.848	1.082
10	0	0.849	1.082

Table 1: Microphone locations. The microphones that are used for model updating are indicated in a bold font.

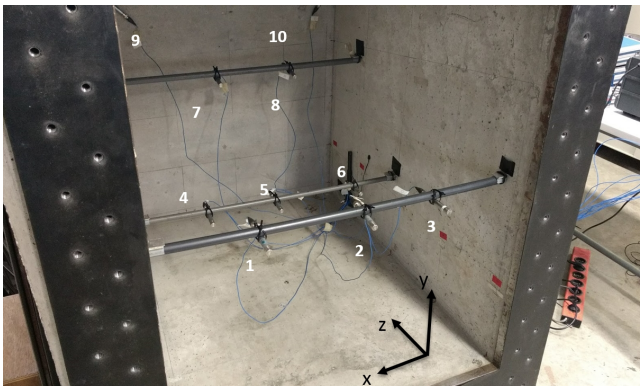

Figure 2: Microphone placement inside the acoustic cavity.

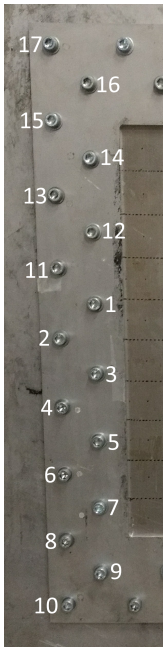

Figure 3: The order in which the bolts were removed from the left hand edge.

4. Example: Structural boundary condition detection with acoustic measurements

The methodology described in Sec. 2 is validated with a vibro-acoustic setup at the KU Leuven, called the SoundBox, which is shown in Fig. 1. Details of this setup can be found in [27]. The setup comprises an aluminum plate of 3 mm thickness attached to an acoustic cavity that is slightly asymmetric. The aluminum plate is clamped between the main frame of the box and the clamping plate by bolts that are all tightened with the same torque of 60 Nm. The goal of the experiment is to detect changes in the structural boundary conditions. This is achieved by progressively removing bolts on the left hand edge, starting from the fully clamped edge until the full edge is free of bolts. The order in which the bolts are removed is indicated in Fig. 3.

Every time a bolt is removed, a new set of FRFs is measured by applying an excitation with an impact hammer. The FRFs are measured at several microphone locations throughout the box, which can be seen in Fig. 2. Also, the microphone locations are given in Table 1.

4.1. Details of the finite element model

For the numerical experiments an FE model is used of which the mesh is shown in Fig. 4. The structural domain is modeled with quadratic triangular shell elements and the acoustic domain is modeled with quadratic tetrahedral elements, leading to a model with 23537 Degrees Of Freedom (DOF). The mesh size is chosen such that the

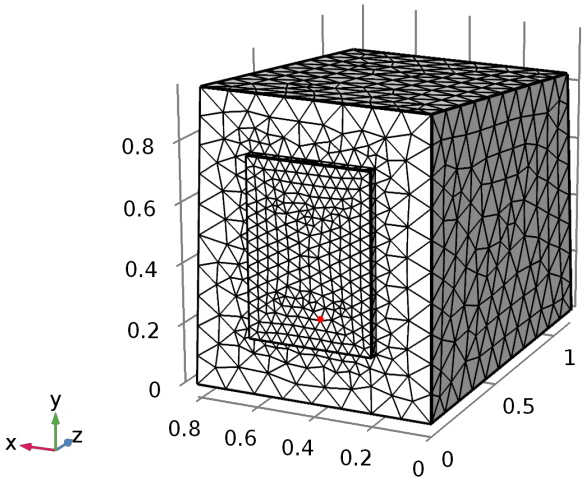

Figure 4: The used Finite Element mesh of the SoundBox, with the excitation point indicated in red.

model is valid until 400 Hz, using the rule of thumb of 10 elements per wavelength. A structural excitation is applied as a point force on $x = 0.2735$ m, $y = 0.3440$ m, $z = -0.035$ m, in the z-direction, which corresponds to the point indicated in red in Fig. 4. To determine the scaling of the structural stiffness matrix, the acoustic mass matrix and the proportional damping coefficients of the plate and the air, a model updating procedure was performed on the reference model, assuming perfectly clamped structural BCs. The details of this procedure can be found in [28] and the resulting parameters that are used in all of the following examples can be found in Table 2. Notice that the plate is modeled with a slightly orthotropic behavior, since it followed from the model updating procedure that this is necessary for an accurate reference model. After identification of the material parameters under nominal conditions, a second model was made in which the left hand edge is supported with a varying rotational stiffness that simulates a simply supported edge (stiffness is zero), a clamped BC (stiffness is infinite) or a BC that is somewhere in between the two. The main assumption here is that the change in the dynamic behavior of the plate due to the removal of the bolts, can be accurately modeled by locally changing the boundary conditions of the numerical model. The varying rotational stiffness of the edge appears on the diagonal of the stiffness matrix and are introduced by summing the nominal (simply supported) stiffness matrix with the local change of the parameter, which is can be modeled with the low-rank affine pMOR approach, shown in Sec. 2. The other edges are modeled with clamped BCs. The acoustic domain is modeled with sound hard boundaries.

The system matrices are extracted from the finite element model and the parameter set that is used in the model updating procedure consists of the rotational edge stiffness of every node along the edge, plus a scaling factor $p^{(damp)}$ for the proportional damping

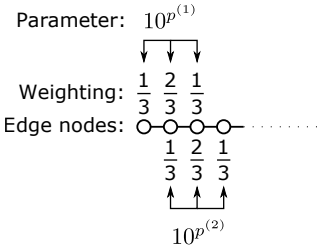

Figure 5: The rotational stiffness is distributed along multiple nodes, to smoothen the stiffness values.

term that works on the whole edge simultaneously, as follows:

$$C(p) = C_0 + 10^{p^{(damp)}} \beta \sum_{i=0}^{\nu} 10^{p^{(i)}} \boldsymbol{b}_i \boldsymbol{c}_i^T, \tag{33}$$

$$C_0 = \alpha M_0, \tag{34}$$

under the assumption that the edge contains ν nodes, and with proportional damping parameters α and β. The scaling factor is introduced to account for the extra damping that occurs due to the imperfect clamped when a few bolts are removed and is multiplied by the change stiffness matrix due to the change in $p^{(i)}$. The proportional damping in the rest of the plate does not change during the optimization procedure. Note that K_0 does not appear in Eq. (34), because this term is zero for the simply supported edge. By using Eq. (19) and (28), and under the assumption of proportional damping, the derivatives of the dynamic stiffness matrix to the parameters become

$$\frac{\partial K_{dyn}(p,\omega)}{\partial p_j} = (\ln(10) i\omega 10^{p^{(damp)}} \beta + \ln(10)) \sum_{i=0}^{\nu} 10^{p^{(i)}} \boldsymbol{b}_i \boldsymbol{c}_i^T. \tag{35}$$

Furthermore, one extra derivative term that describes the derivative of the dynamic stiffness matrix to the damping scaling parameter $p^{(damp)}$ is given as follows:

$$\frac{\partial K_{dyn}(p,\omega)}{\partial p^{(damp)}} = i\omega \ln(10) 10^{p^{(damp)}} \beta \sum_{i=0}^{\nu} 10^{p^{(i)}} \boldsymbol{b}_i \boldsymbol{c}_i^T. \tag{36}$$

The system matrices resulting from the finite element model, including the parameterization, are reduced according to the pMOR method described in Sec. 2. By applying the automatic reduction scheme that has been explained in [29] and which chooses the expansion points and the order of the moment matching procedure, a model of 180 DOF was obtained with a relative error below 0.1 % for all frequencies below 400 Hz. The values of the rotational stiffness were initialized at $p^{(i)} = 4$, which approximates a clamped edge, and the damping scaling parameter at $p^{(damp)} = 0$. This value is chosen, because the resulting FRFs are close to the reference (clamped) FRF, which is required to match the FRFs in the optimization procedure. It was found that even higher values of $p^{(i)}$ leads to ill-conditioned matrices, while not significantly changing the FRFs.

Properties	Symbol	Value
Young's moduli	$E_x,\ E_y,\ E_z$	$66e9,\ 81e9,\ 69E9$ Pa
Poisson's ratios	$\nu_x,\ \nu_y,\ \nu_z$	$0.33,\ 0.33,\ 0.33$
Density plate	ρ	2700 kg/m^3
Thickness	t	0.003 m
Structural damping parameters	$\alpha_s,\ \beta_s$	$5.1357,\ 2.554e-6$
Acoustic damping parameters	$\alpha_a,\ \beta_a$	$3.7755,\ 5.199e-7$
Density air	ρ	1.225 kg/m^3
Acoustic mass scaling factor	δ	0.98179
Structural stiffness scaling factor	γ	0.85361

Table 2: Properties of the updated numerical reference model.

Number of removed bolts	Damping multiplication factor
0 bolts	0.0092
4 bolts	0.2606
6 bolts	1.8705
10 bolts	2.0591
12 bolts	2.5127
15 bolts	3.2690
17 bolts	3.0573

Table 3: Damping multiplication factor $p^{(damp)}$ of the proportional damping term along the edge.

4.2. Results

To improve the conditioning of the system, a Tikhonov regularization term of $\eta = 0.04$ was added to the cost function, as described in Sec. 3. This value was determined by performing an L-curve analysis [21]. Furthermore, because a relatively smooth transition between the stiffness values among neighboring nodes is expected, an additional weighting scheme was applied to the optimization parameters, as shown in Fig. 5. This weighting scheme influences 3 consecutive nodes of the edge, by multiplying $10^{p^{(i)}}$ to 3 weighting factors: The middle node (i) is weighted by 2/3 and the neighboring nodes, $(i-1)$ and $(i+1)$, are weighted by 1/3. The optimization procedure is terminated when the difference between the cost function of two subsequent iterations is less than $1e-3$. The microphones that are used in the optimization procedure are microphone 1, 3, 4, 5, 9, and 10.

4.3. Rotational stiffness estimation

Although no reference stiffness is available to compare the result that follows, it is expected that around the region where the bolts are removed a stiffness decrease will be observed after the model updating procedure is completed. The identified rotational stiffness as function of the amount of bolts removed is shown in Fig. 6. The number of removed bolts are indicated on top of each figure and their locations are indicated with the gray crosses at the bottom of each sub-figure. As can be observed in Fig. 3, these bolts can lie outside of the outer dimensions of the edge. Furthermore, the retrieved damping scaling factor is given in Table 3.

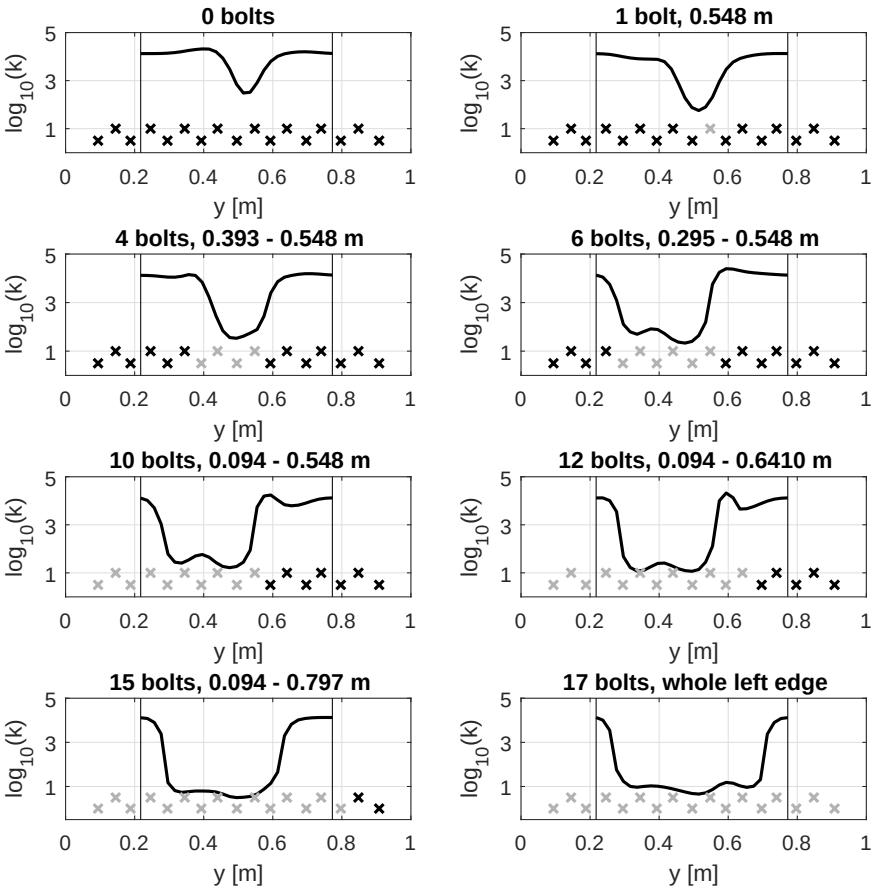

Figure 6: Identified rotational edge stiffness. The tightened bolts are indicated with the black crosses and the removed bolts are indicated in gray.

Process	Full model	Reduced model
One frequency line	0.206 s	0.00239 s
Calculation reduced basis	N/A	417.82 s
Projection reduced model	N/A	100.95 s
Total time	4.90e4 s	575.58 s

Table 4: Time spent on system inversions for full and reduced model, with frequency line 23762 evaluations (needed to converge for 4 removed bolts) and to reduce the model.

The stiffness has been plotted on a logarithmic scale. It can be seen that the location of the removed bolts can be found from the estimated data: The rotational stiffness drops significantly around the region where the bolts are removed. Furthermore, it is observed that the estimated damping scaling factor grows when more bolts are removed, which is expected because of the reduced clamping. The estimation becomes less accurate around the corners of the edge, which can be explained by the influence of the other (still clamped) edges around the corners. There are some fluctuations in the initially identified stiffness (Fig. 6, top left), which has two possible explanations. Firstly, although all bolts are tightened with the same torque, there is no guarantee that the distribution of the resulting clamp is equal across the edge. Secondly, also the change in the dynamic behavior of the plate does not change as much for high stiffness values.

4.4. Comparison of the FRFs

The match between the measured FRFs and the numerical FRF after model updating is shown in Fig. 7 for microphone 1. For the FRFs measured with the other microphone locations similar results are obtained. It can be seen that a good match is obtained for all cases. The importance of adjusting the damping for different boundary conditions can be clearly observed, since for a high number of removed bolts, several resonance peaks are damped out more strongly and this behavior is caught accurately by the model updating procedure.

4.5. Calculation speed of the method

As indicated before, the main reason to use a pMOR model is to speedup the optimization process, such that a detection of anomalies in the BCs can be achieved while performing a measurement campaign. Therefore, the speed of the method is assessed in more detail. In practice, most time is spent on calculating the reduced basis, calculating the FRFs and the subspace projection of the full model to the reduced model. To get an estimate of the amount of time that is required to obtain the same results with the full model, the amount of FRF evaluations were counted for the reduced model and multiplied by the time that is required to calculate one FRF for the full model, see Table 4. The results that are shown here are obtained for the data set with 4 bolts removed. All these calculations were done on a laptop PC with a 2.70 GHz quad-core processor and 16GB of RAM memory. Here, the huge benefit of using parametric reduced order models is clearly visible: While the optimization with the ROM is finished in only a few minutes, the optimization with the full model would take several days.

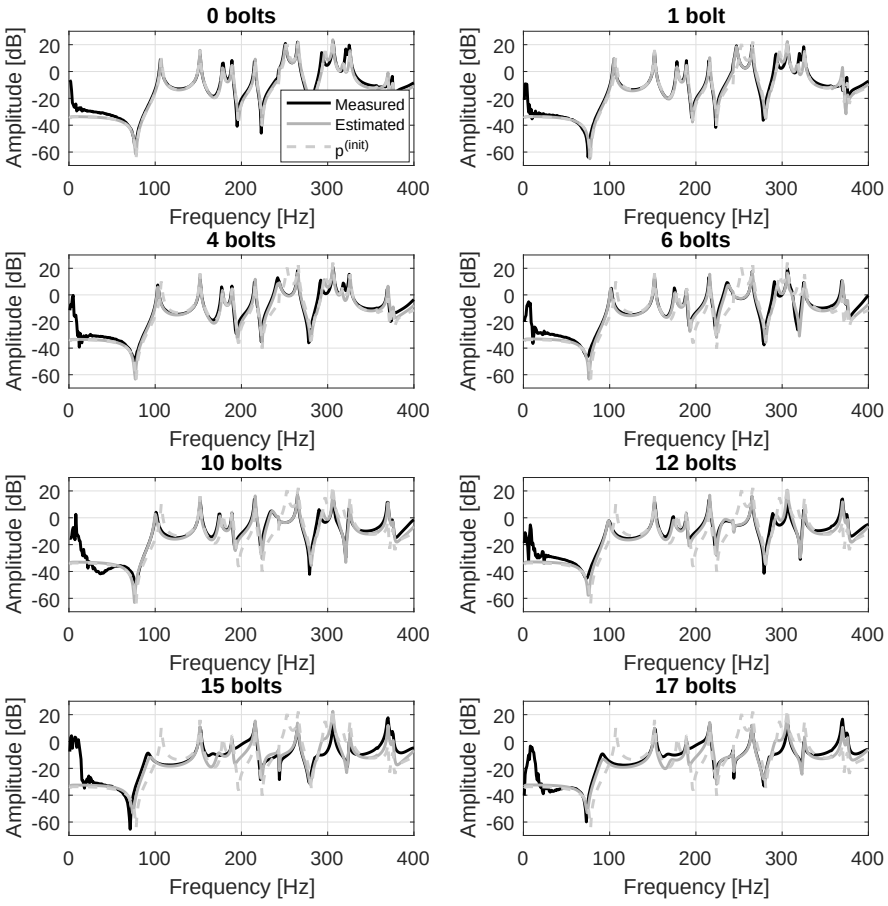

Figure 7: Comparison between the measured FRFs (black) and the estimated FRFs after model updating of the boundary conditions (gray) for microphone 1. The FRF under starting conditions $p^{(init)}$ is shown with the dashed line.

5. Conclusions

A method has been derived that makes it possible to efficiently detect the boundary conditions for linear vibro-acoustic systems. The method works by simulating the parametrized BCs as low-rank changes in the mass, damping and stiffness matrix. By making use of the low-rank characteristics of the model, the system is rewritten so that non-parametric model order reduction techniques can be used to obtain a reduced basis that includes the parametric dependency. This means that, in contrast to pMOR techniques that do not use this low-rank property, the reduction basis is independent of any parameter space sampling, thus a small model is obtained that can be used for fast model updating. Moreover, it is shown that the derivatives of the resulting model can be derived analytically, leading to an additional reduction in the calculation time.

The method is applied on a vibro-acoustic problem, consisting of an aluminum plate that is connected to an acoustic cavity. The plate is clamped to a very thick steel frame by several bolts and these bolts are removed progressively on the left hand edge, to emulate variations in the BCs. The FRFs under the different clamping conditions are measured. Then model updating is applied by updating the rotational stiffness along the edge, plus a scaling factor on the proportional damping in the numerical model. The resulting estimated stiffness clearly indicates possible problem regions and the resulting numerical FRFs match the measurements well. Therefore, it is concluded that this method can be used effectively to determine discrepancies in the BCs between the numerical model and the measurements. Furthermore, the proposed method does this in only a few minutes. This makes it possible to do this assessment for a wide variety of applications: For example, to check the boundary conditions while performing a measurement campaign or quality control of components during assembly.

6. Acknowledgments

The research of S. van Ophem is funded by an Early Stage Researcher grant within the European Project ANTARES Marie Curie Initial Training Network (GA 606817). The research of Axel van de Walle is funded by a Ph.D. grant of the Agency for Innovation by Science and Technology in Flanders (IWT). The research of E. Deckers is funded by a grant from the Fund for Scientific Research, Flanders (F.W.O). The Research Fund KU Leuven is gratefully acknowledged for its support. Furthermore, the authors acknowledge the financial support from Strategic Initiative Materials in Flanders (SIM) through the MADUROS, DEMOPRECI-NDT Program.

Appendix A.

Starting with the cost function itself:

$$C = \log_{10}\left(\sum_{l=1}^{n_{freq}} (T_n^l - T_e^l)^2 + \sum_{k=1}^{\nu} \eta (p^{(k)} - p_{init}^{(k)})^2\right). \tag{A.1}$$

Using the definition of the FRFs as given in Eq. (30) and Eq. (31), and using $H_\bullet = \frac{X_\bullet}{F_\bullet}$, this is rewritten to

$$
\begin{aligned}
C &= \log_{10}\Big(\sum_{l=1}^{n_{freq}} (20\log_{10}(|H_n^l(p)|) - 20\log_{10}(|H_e^l|))^2 + \sum_{k=1}^{\nu} \eta(p^{(k)} - p_{init}^{(k)})^2\Big) \\
&= \log_{10}(A). \qquad \text{(A.2)}
\end{aligned}
$$

Here the variable A is used for ease of notation. By making use of the following definition:

$$
|H_n^l(p)| = \sqrt{[\Re(H_n^l(p))]^2 + [\Im(H_n^l(p)]^2}, \qquad \text{(A.3)}
$$

it is possible to get the derivative by applying the chain rule several times:

$$
\begin{aligned}
\frac{\partial C}{\partial p^{(k)}} = \frac{20(T_n^l - T_e^l)}{ln(10)^2(A)|H_n(p)|^2}(2\Re(H_n(p))\Re[\frac{\partial H_n(p)}{\partial p^{(k)}}] + 2\Im(H_n(p))\Im[\frac{\partial H_n(p)}{\partial p^{(k)}}]) \\
+ \frac{2\eta(p^{(k)} - p_{init}^{(k)})}{ln(10)(A)}. \qquad \text{(A.4)}
\end{aligned}
$$

Because the force is assumed to be parameter independent, the derivatives in Eq. (32) can directly be substituted in Eq. (A.4) to get the full analytical derivative expression.

References

[1] R. D. Cook, D. S. Malkus, M. E. Plesha, R. J. Witt, Concepts and Applications of Finite Element Analysis, fourth edition Edition, Wiley, Madison, 2002.

[2] O. von Estorff, Boundary Elements in Acoustics: Advances and Applications, WITpress, 2000.

[3] J. E. Mottershead, M. I. Friswell, Model Updating In Structural Dynamics: A Survey, Journal of Sound and Vibration 167 (2) (1993) 347–375. doi:10.1006/jsvi.1993.1340.
URL http://www.sciencedirect.com/science/article/pii/S0022460X83713404

[4] J. E. Mottershead, M. Link, M. I. Friswell, The sensitivity method in finite element model updating: A tutorial, Mechanical Systems and Signal Processing 25 (7) (2011) 2275–2296. doi:10.1016/j.ymssp.2010.10.012.
URL http://www.sciencedirect.com/science/article/pii/S0888327010003316

[5] E. M. Hernandez, D. Bernal, Iterative finite element model updating in the time domain, Mechanical Systems and Signal Processing 34 (1) (2013) 39–46. doi:10.1016/j.ymssp.2012.08.007.
URL http://www.sciencedirect.com/science/article/pii/S0888327012003135

[6] D. V. Nehete, S. V. Modak, K. Gupta, Coupled vibro-acoustic model updating using frequency response functions, Mechanical Systems and Signal Processing 7071 (2016) 308–319. doi:10.1016/j.ymssp.2015.09.002.
URL http://www.sciencedirect.com/science/article/pii/S0888327015003970

[7] A. Teughels, G. De Roeck, J. Suykens, Global optimization by coupled local minimizers and its application to FE model updating, Computers & Structures 81 (2003) 2337–2351.

[8] V. K. Balla, L. Coox, E. Deckers, B. Pluymers, W. Desmet, K. Marudachalam, Obtaining manufactured geometries of deep-drawn components through a model updating procedure using geometric shape parameters, Mechanical Systems and Signal Processing 98 (Supplement C) (2018) 382–401. doi:10.1016/j.ymssp.2017.05.009.
URL http://www.sciencedirect.com/science/article/pii/S0888327017302613

[9] W. Heylen, S. Lammens, P. Sas, Modal Analysis Theory and Testing, KU Leuven, Department mechanical engineering, 2012.

[10] B. Moore, Principal component analysis in linear systems: Controllability, observability, and model reduction, IEEE Transactions on Automatic Control 26 (1) (1981) 17–32. doi:10.1109/TAC.1981.1102568.

[11] C. W. Rowley, Model reduction for fluids, using balanced proper orthogonal decomposition, International Journal of Bifurcation and Chaos 15 (03) (2005) 997–1013. doi:10.1142/S0218127405012429.
URL http://www.worldscientific.com/doi/abs/10.1142/S0218127405012429
[12] Z. Bai, Y. Su, Dimension Reduction of Large-Scale Second-Order Dynamical Systems via a Second-Order Arnoldi Method, SIAM Journal on Scientific Computing 26 (5) (2005) 1692–1709. doi:10.1137/040605552.
[13] E. J. Grimme, Krylov Projection Methods for Model Reduction, Ph.D. thesis, University of Illinois, Illinois (1997).
[14] A. van de Walle, F. Naets, E. Deckers, W. Desmet, Stability-preserving model order reduction for time-domain simulation of vibro-acoustic FE models, International Journal for Numerical Methods in Engineering. 109 (6) (2017) 889–912. doi:10.1002/nme.5323.
URL http://onlinelibrary.wiley.com/doi/10.1002/nme.5323/abstract
[15] S. van Ophem, O. Atak, E. Deckers, W. Desmet, Stable model order reduction for time-domain exterior vibro-acoustic finite element simulations, Computer Methods in Applied Mechanics and Engineering 325 (2017) 240–264.
URL http://www.sciencedirect.com/science/article/pii/S0045782516310659
[16] P. Benner, S. Gugercin, K. Willcox, A Survey of Projection-Based Model Reduction Methods for Parametric Dynamical Systems, SIAM Review 57 (4) (2015) 483–531. doi:10.1137/130932715.
URL http://epubs.siam.org/doi/abs/10.1137/130932715
[17] Y. Yue, K. Meerbergen, Parametric model order reduction of damped mechanical systems via the block Arnoldi process, Applied Mathematics Letters 26 (6) (2013) 643–648. doi:10.1016/j.aml.2013.01.006.
URL http://www.sciencedirect.com/science/article/pii/S0893965913000335
[18] U. Baur, C. Beattie, P. Benner, Mapping parameters across system boundaries: parameterized model reduction with low rank variability in dynamics, Proceedings in Applied Mathematics and Mechanics 14 (1) (2014) 19–22. doi:10.1002/pamm.201410006.
URL http://onlinelibrary.wiley.com/doi/10.1002/pamm.201410006/abstract
[19] S. van Ophem, E. Deckers, W. Desmet, Parametric model order reduction without a-priori sampling for low rank changes in vibro-acoustic systems, Under review for publication in Mechanical Systems and Signal Processing (2017).
[20] L. Van Belle, D. Brandolisio, E. Deckers, S. Jonckheere, C. Claeys, B. Pluymers, W. Desmet, Experimental validation of numerical structural dynamic models for metal plate joining techniques, Journal of Vibration and Control (2017) 1077546317704794doi:10.1177/1077546317704794.
URL https://doi.org/10.1177/1077546317704794
[21] D. Calvetti, S. Morigi, L. Reichel, F. Sgallari, Tikhonov regularization and the L-curve for large discrete ill-posed problems, Journal of Computational and Applied Mathematics 123 (1) (2000) 423–446. doi:10.1016/S0377-0427(00)00414-3.
URL http://www.sciencedirect.com/science/article/pii/S0377042700004143
[22] L. Rouleau, B. Pluymers, W. Desmet, Characterisation of viscoelastic layers in sandwich panels through inverse techniques, in: Proceedings of NOVEM 2015, Dubrovnik, Croatia, 2015.
[23] A. van de Walle, L. Rouleau, E. Deckers, W. Desmet, Parametric model-order reduction for viscoelastic finite element models: an application to material parameter identification, in: Proceedings of the 22nd International Congress on Sound and Vibration, Florence, Italy, 2015.
[24] R. Fletcher, Practical methods of optimization, 2nd Edition, John Wiley & Sons, New York, 1987.
[25] L. Armijo, Minimization of functions having Lipschitz continuous first partial derivatives, Pacific Journal of Mathematics 16 (1) (1966) 1–3.
URL https://msp.org/pjm/1966/16-1/p01.xhtml
[26] K. Choi, N. Kim, Structural Sensitivity Analysis and Optimization 1: Linear Systems, Springer, 2005.
[27] M. Vivolo, Vibro-acoustic Characterization of Lightweight Panels by using a Small Cabin, Ph.D. thesis, KU Leuven (Aug. 2013).
[28] K. Komori, A. van de Walle, T. Toi, W. Desmet, Parameter identification for vibro-acoustic systems by using parametric model order reduction, in: Proceedings of Internoise 2017, Hong Kong, 2017.
[29] A. van de Walle, The power of model order reduction in vibroacoustics and its applications in model-based sensing, PhD thesis, KU Leuven (Jan. 2018).